HHS Public Access

Author manuscript

Acta Biomater. Author manuscript; available in PMC 2018 August 01.

Published in final edited form as:

Acta Biomater. 2017 August ; 58: 254–268. doi:10.1016/j.actbio.2017.06.006.

Angle-ply biomaterial scaffold for annulus fibrosus repair replicates native tissue mechanical properties, restores spinal kinematics, and supports cell viability

Ryan Borem[a], **Allison Madeline**[a], **Joshua Walters**[a], **Henry Mayo**[a], **Sanjitpal Gill**[a,b], and **Jeremy Mercuri**[a,*]

[a]The Laboratory of Orthopaedic Tissue Regeneration & Orthobiologics, Department of Bioengineering, Clemson University, Clemson, SC, USA

[b]Department of Orthopaedic Surgery, Medical Group of the Carolinas-Pelham, Spartanburg Regional Healthcare System, Greer, SC, USA

Abstract

Annulus fibrosus (AF) damage commonly occurs due to intervertebral disc (IVD) degeneration/herniation. The dynamic mechanical role of the AF is essential for proper IVD function and thus it is imperative that biomaterials developed to repair the AF withstand the mechanical rigors of the native tissue. Furthermore, these biomaterials must resist accelerated degradation within the proteolytic environment of degenerate IVDs while supporting integration with host tissue. We have previously reported a novel approach for developing collagen-based, multi-laminate AF repair patches (AFRPs) that mimic the angle-ply architecture and basic tensile properties of the human AF. Herein, we further evaluate AFRPs for their: tensile fatigue and impact burst strength, IVD attachment strength, and contribution to functional spinal unit (FSU) kinematics following IVD repair. Additionally, AFRP resistance to collagenase degradation and cytocompatibility were assessed following chemical crosslinking. In summary, AFRPs demonstrated enhanced durability at high applied stress amplitudes compared to human AF and withstood radially-directed biaxial stresses commonly borne by the native tissue prior to failure/detachment from IVDs. Moreover, FSUs repaired with AFRPs and nucleus pulposus (NP) surrogates had their axial kinematic parameters restored to intact levels. Finally, carbodiimide crosslinked AFRPs resisted accelerated collagenase digestion without detrimentally effecting AFRP tensile properties or cytocompatibility. Taken together, AFRPs demonstrate the mechanical robustness and enzymatic stability required for implantation into the damaged/degenerate IVD while supporting AF cell infiltration and viability.

Keywords

Annulus fibrosus; Angle-ply laminate; Collagen scaffold; Tissue engineering; Intervertebral disc

*Corresponding author at: 313 Rhodes Engineering Research Center, Clemson, SC, USA. jmercur@clemson.edu (J. Mercuri).

1. Introduction

Intervertebral discs (IVD) support axial compressive loading of the spine while allowing for flexibility and a defined range of motion during activities of daily living. IVD's are comprised of two distinct regions: the central gelatinous core known as the nucleus pulposus (NP) which is circumferentially constrained by the annulus fibrosus (AF). The NP is a highly-hydrated tissue composed primarily of collagen type II and aggrecan, which provides load support due to its low permeability and the generation of intradiscal pressure (IDP). The AF is a highly organized lamellar structure consisting of 15–25 sheets of collagen type I with fibers aligned in alternating orientations of ±28–43° to the transverse axis of the spine yielding an 'angle-ply' architecture [1]. The AF functions to circumferentially confine the NP and resist tensile strains experienced during rotational and bending spinal motions [2,3].

Annually, over 5.7 million Americans are diagnosed with IVD disorders including IVD degeneration (IVDD) and herniation (IVDH) which ultimately compromise the structural integrity of the AF [4]. This results in a loss of IVD height, impaired IVD mechanical function, patient pain, and disability [5–11]. Accordingly, discogenic low back pain (LBP) affects approximately 80% of the adult population during their lifetime resulting in a diminished quality of life [4,12–14], and estimated healthcare expenditures exceeding $85.9 billion [15,16]. Surgical treatments for late-stage IVDD include spinal fusion and total disc replacement, however these methods suffer from significant drawbacks [17]. Newer technologies, including NP replacement (NPR) are being developed as interventional strategies to mitigate IVDD progression [18,19]. Such devices have not yet realized clinical utility, due in part to the lack of a mechanically robust AF repair method. Additionally, the nearly 500,000 patients undergoing discectomies annually to remove protruding/herniated NP tissue may benefit from a biomaterial that can restore AF integrity following the procedure. Studies demonstrate that conservative discectomies (i.e. those removing minimal NP material) often result in maintenance of IVD height, biomechanics and improved patient outcomes; however these patients are at increased risk for re-herniation, and incur significant reoperation costs [20–29]. These detrimental consequences may be moderated via utilization of an AF repair method.

Accordingly, there has been a recent increase in the development of AF repair strategies ranging from simple mechanical closures to biomaterial scaffolds. While many biomaterials developed for AF repair have been assessed for their ability to promote tissue regeneration *in vitro* [30–34], few have undergone thorough testing to evaluate their mechanical competency required for implantation into the spine [34–37]. Moreover, even fewer have been assessed for their contribution to restoring functional spinal unit (FSU) kinematics following injury and repair; arguably one of the most important functional outcomes of any motion preserving/sparing spinal implant. Finally, biomaterials to be implanted into a damaged IVD must demonstrate resistance to accelerated degradation as investigations have illustrated increased concentrations of destructive proteases which could jeopardize their mechanical integrity [38–40]. This is of particular importance for biomaterials composed of extracellular matrix (ECM) components, which often have to be chemically crosslinked to impart resistance to accelerated enzymatic degradation, yet should demonstrate cytocompatibility. Taken together, a critical need exists to create an effective AF repair biomaterial, which

demonstrates the ability to survive in the mechanical, and biochemical environment of the damaged IVD and which will allow for eventual integration or regeneration of healthy AF tissue. The development of such a biomaterial may reduce the rate of IVD re-herniation, improve patient outcomes, and delay the need for spinal fusion procedures [41].

We have previously reported the development of a novel collagen sheet-based annulus fibrosus repair patch (AFRP) biomaterial derived from decellularized porcine pericardium, which has been assembled using a simple, scalable, and repeatable process. The resulting AFRPs have been shown to mimic the multi-laminate angle-ply (i.e. layered) architecture and basic tensile mechanical properties of the human AF [42]. Herein we aimed to further mechanically evaluate this biomaterial for its tensile fatigue strength, resistance to impact loading, attachment strength to IVDs, and its ability to assist in restoring axial kinematics following repair of injured FSUs. Additionally, we have assessed the ability of various crosslinking chemistries to render AFRPs resistant to accelerated protease degradation and evaluated their effects on AFRP tensile properties. Finally, considering the long-term goal of using this biomaterial in conjunction with autologous or allogenic cells to regenerate healthy AF tissue, we evaluated the ability of the AFRP to support AF cell viability and infiltration.

2. Materials & methods

2.1. Fabrication of annulus fibrosus repair patches (AFRPs)

Multi-laminate angle-ply AFRPs were developed and assembled from decellularized porcine pericardium as previously described by McGuire et al. [42]. AFRPs were maintained in a phosphate buffered saline storage solution containing protease inhibitor at 4 °C for up to two weeks prior to testing.

2.2. Preparation of functional spinal units

Bovine tails from 2 to 3-year-old calves were obtained from a local abattoir and transported on wet ice to the lab within an hour. Excess tissue surrounding the vertebral bodies and intervertebral discs were removed via dissection and functional spinal units (FSUs: vertebrae-IVD-vertebrae) were isolated via shears. Three FSUs were harvested from three caudal levels (cc1-2 to cc3-4: IVDs closest to the rear end) and were potted using wood screws and urethane potting resin to prevent slippage of the samples during testing. In general, bovine IVDs have been shown to have similar swelling pressure, geometry and resting stress compared to human lumbar IVDs [43]. Prior to testing, FSUs were wrapped in gauze saturated with storage solution and stored at −20 °C. Samples were thawed within the sealed zip-lock bag, which was submerged for four hours in PBS at ambient temperature thus not allowing tissue swelling.

2.3. Biomechanical evaluations of non-crosslinked multi-laminate AFRPs

2.3.1. Biaxial impact burst strength of AFRPS—Biaxial impact burst strength testing was modeled after ASTM D1709: “Standard Test Methods for Impact Resistance of Plastic Film by the Free-Falling Dart Method” with modification. Representative samples of AFRPs (2-, 3-, and 6-ply; n = 5/group; AFRP dimensions: 2-ply; 12 mm (L) × 12 mm (W) × 0.5 mm (T), 3-ply; 12 mm (L) × 12 mm (W) × 0.75 mm (T), 6-ply: 12 mm (L) × 12 mm (W) × 1.5

mm (T)) were tested using a custom designed free-fall impact testing drop-tower (Supplemental Fig. 1A). The base platform of the drop-tower consisted of a tissue holding clamp and four vertical rails, which guided a free-falling platform. The tissue holding apparatus consisted of two stacked blocks lined with course-grit sandpaper each having an aligned thru-hole of 6.25 mm diameter. AFRPs were sandwiched between the two blocks centered over the two thru-holes. Subsequently, a 6 mm steel ball attached to a 3-inch pushrod was placed in contact with the AFRP via the thru-hole in the superior block. Various weights ranging from 0.18 to 0.58 kg were stacked on the free-fall platform, which were then dropped from a constant height of 0.254 m. Impact energy (E) was calculated using the equation for kinetic energy, $E=\frac{1}{2}*m*v^2$, where m = mass and v = velocity. The resultant ball-burst pressure was calculated given the maximum force at rupture and its relationship with ball-burst pressure and geometric constraints according to established procedures [42,44,45]. AFRPs were kept moist throughout testing via saline spray.

2.3.2. Tensile fatigue strength of AFRPs—Tensile testing was performed using the methods described by Green et al. with minor modification [46]. Testing was performed using a Bose ElectroForce 3200 series (model 3220), fitted with a 100-lb. load cell in test chamber filled with PBS and protease inhibitor solution at ambient temperature. Three-ply AFRPs (n = 16; AFRP dimensions: 7 mm (L) × 7 mm (W) × 0.75 mm (T)) were pre-conditioned using 5 cycles of 10% strain applied at a rate of 10 mm/min prior to initiation of fatigue testing. Varying stress amplitudes ranging from 0.95 to 2.66 MPa (i.e. stress values typically observed in the lumbar spine during activities of daily living [46]) were applied at a frequency of 0.5 Hz; the number of cycles to failure at each applied stress for each sample was recorded and plotted to develop an S-N curve. Testing was stopped if failure did not occur prior to achieving 10,000 loading cycles, which was defined as a run-out. Displacement, load, total testing time, cycle count, and location of material failure were recorded for all samples.

2.3.3. Strength of non-crosslinked AFRP attachment to IVDs—The strength of attachment of the AFRP to the IVDs was performed using a ball-burst test modeled after ASTM D3786/D3786M: “Standard Test Method for Bursting Strength of Textile Fabrics – Diaphragm Bursting Strength Tester Method” with modification (Supplemental Fig. 1B). Laterally directed thru-holes were drilled through the center of bovine tail IVDs using a 6.25 mm drill bit to simulate a large herniation or implantation pathway for a pre-formed NPR. AFRP’s (n = 6; AFRP dimensions: 7 mm (L) × 7 mm (W) × 0.75 mm (T)) were then secured to the FSUs over the center of the defect. Attachment included that application of a topical adhesive (Dermabond Advanced) to temporarily secure the AFRP while it was being sutured (4–0 FiberWire; Arthrex) in place at the four corners of the AFRP with the suture inserted 1– 2 mm from the edge of the AFRP with throws directed perpendicular to the surface of the AF tissue. Testing was performed on an Instron mechanical testing system with a 1000 N load cell. A 3-inch long pushrod with a 6 mm steel ball was placed in the Instron’s upper grip and force was directed radially through the IVD and perpendicular to AFRP (i.e. load was applied perpendicular to collagen fiber alignment in the AFRP similar to radial forces applied to the native intact AF by the NP) at a constant rate of 300 mm/min.

Displacement and load were recorded until failure of the attachment occurred, and the resultant ball-burst pressure was calculated given the maximum force at rupture and its relationship with ball-burst pressure according to established equations [42,44,45]. AFRPs were kept moist throughout testing via saline spray.

2.4. FSU kinematic testing following repair with non-crosslinked AFRPs and NPRs

Axial kinematic testing was performed on a Bose ElectroForce 3200 series, model: 3220, fitted with a 100-lb. load cell in a test chamber filled with PBS and protease inhibitor solution at ambient temperature. The loading methodology and analysis were adapted from previous reports [33,36]. Briefly, each FSU (n = 5) was tested sequentially as follows: Intact, Annulotomy, Discectomy, and Repair (Fig. 1A). An annulotomy was performed by perforation of the IVD using a 6 mm biopsy punch (7 mm depth) and the subsequent removal of the AF tissue. Aggressive discectomy was performed by removing 1.0 ± 0.2 mL of NP tissue through the previously formed aperture remaining after annulotomy. The repair group consisted of replacing the excised tissue with an equal volume of a biologic NPR (termed ABNP – developed and described previously by our lab [19]) prior to closure with the AFRP (n = 5; AFRP dimensions: 7 mm (L) × 7 mm (W) × 0.75 mm (T)) which was secured initially with topical adhesive prior to suturing. Suturing of the AFRP consisted four corner suturing with sutures being passed through the AFRP 1–2 mm from the edge of the AFRP with throws directed in alignment with the ±30° collagen fibrils in the AFRP such that the fibers were captured within the knot. Prior to test initiation, samples were preloaded to a mean stress of −0.125 MPa; a physiologically relevant stress magnitude borne by the IVD *in vivo*. Between each test, IVD samples were equilibrated in the saline bath for approximately 5 min before test initiation. FSUs were then subjected to three consecutive loading regimes: 1) a 1-h creep period at −0.5 MPa, 2) immediately followed by 35 cycles of tension-compression between 0.25 MPa and −0.5 MPa at 0.1 Hz, and 3) ending with a constant slow-ramp to −0.5 MPa at a rate of 1 N/s. The testing rate of 0.1 Hz has been shown to represent normal physiological spinal frequency (Fig. 1B) [33,47].

The force-displacement curve (Fig. 1C) for the unloading phase of the 35th cycle was used to analyze the cyclic loading data as previously described to ensure dynamic equilibrium was achieved [36]. Tensile and compressive stiffness were calculated via linear fit of the force-displacement curve from 60% to 100% of the respective peak loads. Axial range of motion (RoM) was defined as the total peak-to-peak displacement of the IVD. Neutral zone (NZ) length was determined by fitting a third-order polynomial to the data and finding the maxima and minima with the correlating range between the peaks. Creep data (Fig. 1D) was analyzed using a non-linear constitutive model fit to the data using R statistical software as described previously [36]. Step displacement was defined as the initial deformation that occurred until the target load was achieved, while the creep displacement was the displacement that occurred after the step displacement. A four-parameter rheological model equation: $\frac{d(t)}{L_o}=\frac{1}{\Psi_1}\left(1-e^{\frac{-t\Psi_1}{\eta_1}}\right)+\frac{1}{\Psi_2}\left(1-e^{\frac{-t\Psi_2}{\eta_2}}\right)$ was fit to the creep displacement data, where Ψ_i represents the elastic response and η_i represents the viscous response. Short-term and long-term creep time constants (τ_1 and τ_2, respectively) were derived from constitutive

model coefficients using the equation: $\tau_i = \frac{\Psi_i}{\eta_i}$. The constant-rate slow-ramp compression stiffness was determined using a linear fit of the slow-ramp load-displacement response.

2.4.1. Compression to failure of FSUs repaired with non-crosslinked AFRPs and NPRs—Following kinematic testing of FSUs, samples were transferred to an Instron mechanical testing system fitted with a 10kN load cell. Samples were compressed to failure at a rate of 300 mm/min until FSU failure (i.e. contact of the adjacent vertebral end plates and/or AFRP failure/NPR herniation). Sample load and initial cross-sectional area of the IVDs were determined to calculate the engineering compressive stress applied to the IVD. Digital video was used to record mode and time of failure (Supplemental Video).

2.5. AFRP crosslinking studies

2.5.1. crosslinking procedures—Crosslinking of AFRPs using various concentrations of either carbodiimide-or glutaraldehyde-based chemistries were evaluated. Carbodiimide-based crosslinking was carried out using either 6 mM or 30 mM 1-Ethyl-3-(3-dimethylaminopropyl) Carbodiimide HCl (EDC) with 1.2 mM or 6 mM N-hydroxysuccinimide (NHS), respectively while buffered in 50 mM 2-(N-morpholino) ethanesulfonic acid (MES) (pH 5.5) at ambient temperature. Glutaraldehyde (GLUT) treated AFRPs were prepared using 0.2% or 0.6% GLUT in 50 mM 4-(2-hydroxyetheyl)-1-piperazineethanesulfonic acid (HEPES) buffer (pH 7.4) at ambient temperature. Following 24 h of crosslinking, all AFRPs were rinsed and placed in storage solution for a maximum of 3 days at 4 °C prior to testing.

2.5.2. Collagen stability of crosslinked AFRPs—Thermal denaturation temperature (T_d) was used as a measure of collagen stability of non-crosslinked and crosslinked (6 mM and 30 mM EDC, 0.2% and 0.6% GLUT) AFRPs in addition to native bovine AF tissue for comparison (n = 3 non-crosslinked AFRPs and fresh AF) (n = 4/crosslinked group). Briefly, a differential scanning calorimeter (DSC: Model Q1000) was used to determine T_d which was defined as the maximum value of the endothermic peak (thermal transition midpoint). Heating of each sample was performed from 20 to 120 °C at a rate of 10 °C/minute in accordance with previous literature [48,49].

2.5.3. Crosslinked AFRP resistance to accelerated collagenase degradation—The resistance to accelerated collagenase degradation was assessed for non-crosslinked and crosslinked (6 mM and 30 mM EDC, 0.2% and 0.6% GLUT) AFRPs (n = 5/group) in addition to native bovine AF tissue (n = 3/group per time point). Samples were rinsed in TRIS buffer, blotted dry, frozen at −80 °C, lyophilized, weighed, and rehydrated in TRIS buffer. Samples were then incubated in 2 mL of 33.6 U/mL collagenase type I at 37 °C for up to 7 days. Sample mass loss was determined by comparing the dry mass of each sample before and after enzymatic digestion. At Day 7, samples were further incubated for an additional 7 days in an increased concentration of collagenase, 336 U/mL, to ensure full tissue degradation.

2.5.4. Tensile properties of crosslinked AFRPs—To define the effect of crosslinking on AFRPs, tensile testing was performed using an MTS mechanical system using methods previously described by Green et al. with minor modification [46]. Crosslinked AFRPs (n = 5/group; AFRP dimensions: 14 mm (L) × 14 mm (W) × 0.75 mm (T)) were affixed between two tensile grips such that the fiber alignment of the AFRPs was oriented ±30° to the axis of applied tension. AFRPs were preconditioned for 5 cycles to 10% strain at 10 mm/min and tested to failure at 240 mm/min to determine elastic modulus (EM: linear region of the stress-strain curve), ultimate tensile strength (UTS: maximum peak load divided by the initial cross-sectional area of the sample) and maximum tensile strain at failure (TSF: % strain at AFRP failure).

2.6. Cell seeding studies on crosslinked AFRPs

2.6.1. Isolation and expansion of bovine AF cells—Primary bovine AF cells (bAFCs) were enzymatically isolated from freshly isolated bovine tail caudal IVDs (n = 4 IVDs from different donors). Briefly, the NP was removed first via an 8 mm biopsy punch to ensure harvest of only AF tissue. The AF tissue was then removed, minced via scalpel, and transferred to a 50 mL conical tube with 25 mL of collagenase solution (1% Ab/Am, 0.2% Collagenase Type I (125 units/mg) and Dulbecco's Modified Eagle Medium (DMEM). Following overnight (~18 h) digestion at 37 °C, and the digested tissue was filtered through a 100 μm cell strainer and the filtered cell suspension was centrifuged at 1000 rpm for 5 min. The supernatant was removed and the cells were re-suspended in cell culture media (CCM), pooled and expanded. CCM consisted of DMEM (with L-glutamine, 1 g/l glucose and sodium pyruvate) containing 10% fetal bovine serum (FBS) and 1% antibiotic/antimycotic (Ab/Am). Passage 3 (P3) bAFCs were used for all studies.

2.6.2. Preperation and seeding of crosslinked AFRPs—Prior to cell seeding, all AFRPs (n = 5/group; AFRP dimensions: 7 mm (L) × 7 mm (W) × 0.75 mm (T)) were sterilized in 0.1% neutral buffered (pH 7.4) peracetic acid for two hours on an orbital shaker at 150 rpm, rinsed in sterile PBS (3×: 1 h/wash), and neutralized (50% FBS/48% DMEM +2% Ab/Am) while agitated on an orbital shaker at 150 rpm at ambient temperature. AFRPs were then seeded on the surface of each ply with bAFCs (9×10^6 cells/cm^3) via dropwise addition. To cell seed the surface of the interior ply, a 21*G* needle was used to puncture through the edge of the AFRP immediately adjacent to the suture line and cells were injected. Cell seeded AFRPs were cultured under standard culture conditions at 37 °C for up to 14 days.

2.6.3. Cytocompatbility of crosslinked AFRPs—Cytotoxicity of crosslinked AFRPs was assessed following bAFC seeding via a lactate dehydrogenase assay (LDH; n = 3/time-point/group) performed on the CCM. Positive death controls consisted of AFRPs seeded with bAFCs, which were allowed to culture in parallel with the experimental groups. Subsequently, three days prior to LDH analysis on crosslinked AFRPs, the corresponding positive death controls were snap frozen and placed back in culture for the remainder of three days so LDH could accumulate. LDH values are expressed as a percentage of the positive (100%) cell death control.

2.6.4. Cell infiltration into crosslinked AFRPs—To determine the effect of AFRP crosslinking on bAFC infiltration depth, histological analysis was used to quantify cell infiltration and distribution on 3-ply AFRPs (n = 5/group; AFRP dimensions: 7 mm (L) × 7 mm (W) × 0.75 mm (T)). Following seeding and culture, AFRPs were fixed in 10% neutral buffered formalin for 24 h prior to paraffin embedding and sectioning to 5 μm followed by staining with Hematoxylin and Eosin (H&E). A Zeiss Axio Vert.A1 microscope with AxioVision SE64 Rel. 4.9.1 software was used for imaging slides. Additionally, ImageJ 1.50b software was used to quantitatively define cellular infiltration depth via imaging three random locations per AFRP (n = 3/group) at 200 × total magnification and averaging the bAFC infiltration depth of the 20 deepest cell nuclei from the outer edge of the respective ply.

2.6.5. Sonication of crosslinked AFRPs—To determine if sonication would assist in improving bAFC infiltration depth into crosslinked AFRPs, a Branson ultrasonic cleaner (model 2800; 40 kHz) was used to physically disrupt 6 mM EDC crosslinked AFRPs for 1-, 5-, and 10-min, respectively.

2.6.6. Tensile properties of crosslinked & sonicated AFRPs—To define the effect of sonication on mechanical properties of 6 mM EDC crosslinked AFRPs (n = 5/group), tensile testing was performed as outlined above in section 2.5.4.

2.6.7. Cell infiltration into crosslinked & sonicated AFRPs—To define the effect of sonication on cell infiltration within 6 mM EDC crosslinked AFRPs (n = 5/per group), histological analysis was performed as outlined above in section 2.6.4.

2.7. Statistical analysis

Statistical analysis of the data was performed using GraphPad Prism 7 software. Results are represented as mean ± standard error of the mean (SEM) and were statistically compared via a one-way ANOVA followed by a Tukey's (Biaxial Impact Burst Strength, Tensile Fatigue Strength, IVD Attachment Strength, and Compression to Failure) or Dunnet's (Collagen Stability, Resistance to Collagenase Degradation, Cytocompatibility-LDH Assay, Cell Infiltration, and Tensile Properties of Crosslinked and Sonicated AFRPs) post hoc statistical analyses. FSU kinematic data was evaluated with a one-way repeated measures ANOVA followed by Dunnet's post hoc analysis. Significance was defined as ($p < 0.05$).

3. Results

3.1. Non-crosslinked AFRPs withstand physiologically relevent impact stresses

Multi-laminate AFRPs underwent biaxial impact burst strength to evaluate its resistance to failure during sudden changes in IDP. Mean burst strength of 2-, 3-, and 6-ply AFRPs was 0.94 ± 0.01 MPa, 1.51 ± 0.06 MPa, and 3.42 ± 0.09 MPa, respectively (Fig. 2A). Additionally, the average kinetic energy absorbed by 2-, 3-, and 6-ply AFRPs was 0.32 ± 0.003 J, 0.51 ± 0.02 J, and 1.16 ± 0.03 J, respectively. Expectedly, burst strength increased with increasing number of plies; the burst strength of 6-ply AFRPs was statistically greater than 2-($p = 0.0003$) and 3-ply ($p = 0.0006$) AFRPs.

3.2. Non-crosslinked AFRPs fatigue strength IS comparable to human AF tissue

Tensile fatigue failure was evaluated to determine the endurance limit of AFRPs by measuring the cycles to failure across three different applied stress amplitude ranges (low: 1.5–2 MPa, moderate: 2–2.5 MPa, and high: 2.5–3 MPa) which represent 25–80% of the UTS range of native posterolateral human AF (Fig. 2B) [46]. The average number of cycles to failure when exposed to low and moderate stress amplitude ranges for AFRPs was 6932 ± 946 and 4068 ± 1055 cycles, respectively which were not statistically different from the number of cycles to failure reported for native human AF tissue (7959 ± 2041 and 2536 ± 1076 cycles, respectively). However, at higher applied stress amplitudes, the number of cycles endured prior to failure by AFRPs (1155 ± 75 cycles) was significantly greater ($p = 0.0443$) compared to native human AF tissue (447.5 ± 252.5 cycles).

3.3. Attachment of non-crosslinked AFRPs to IVDs can resist physiologically relevant pressures

The attachment strength of 3-ply AFRPs following suturing to bovine tail caudal IVDs was determined using a modified ball-burst test. The average biaxial attachment strength of 3-ply AFRPs was 1.45 ± 0.08 MPa (Fig. 3). Macroscopic evaluation of AFRPs following testing illustrated three primary failure modes: AFRP rupture (1 of 6 AFRPs), failure by suture break (4 of 6 AFRPs), and a combination of suture breakage and AFRP rupture (1 of 6 AFRPs) (Fig. 3G–I). Together, these results illustrated that the 4–0 suture used to attach the AFRP commonly failed prior to the AFRP itself. The UTS of a single loop of suture was also determined to be 21.24 ± 1.87 N via suture pull-out strength testing from a 3-ply; no AFRP failure occurred during these tests again confirming that the suture was primary failure location.

3.4. Non-crosslinked AFRPs contirbute to the restoration of FSU kinematics

Following injury (i.e. aggressive annulotomy and discectomy) of bovine caudal IVDs, changes were noted in each mechanical testing parameter evaluated. Results were subsequently normalized to the corresponding intact control; these ratios are shown in Fig. 4. In summary, implantation of both the ABNP and the AFRP demonstrated their ability to restore most mechanical parameters to intact values (Tables 1 and 2). A representative axial force-displacement curve from the cyclic tension-compression testing are shown in (Fig. 1C). Cyclic testing demonstrated a significant increase ($p = 0.0475$) in the range of motion (RoM) between the discectomy (4.62 ± 0.18 mm) and intact groups (4.18 ± 0.17 mm); however, the RoM was restored to intact levels following implantation of the AFRP and ABNP (4.42 ± 0.2 mm; $p > 0.05$) as was indicated by a lack of statistical difference comparing between the two groups. Furthermore, trends towards achieving restoration to intact values of compressive and tensile stiffness values and neutral zone length (NZ) (intact: 1120.9 ± 48.6 MPa, 319.6 ± 31.0 MPa, and 1.63 ± 0.1 mm, respectively) were observed in the group repaired with AFRP and ABNP (1093.2 ± 44.0 MPa, 315.79 ± 20.6 MPa, and 1.74 ± 0.1 mm, respectively). Slow ramp compressive stiffness of the intact FSUs (527.2 ± 20.9 MPa) demonstrated a significant decrease ($p = 0.0001$) following discectomy (325.0 ± 12.9 MPa); however the compressive stiffness following annulotomy and repair (412.13 ± 46.7

MPa and 350.7 ± 52.7 MPa, respectively) were not statistically different compared to the intact condition thus indicating restoration.

A representative creep rate curve was determined from the average curve fit parameters of the test groups developed from a four-parameter exponential model as shown in (Fig. 1D). The overall step displacement followed a graded response with the largest step displacement observed in the discectomy group (2.89 ± 0.46 mm). This large step displacement was associated with the subsequent statistically smaller ($p = 0.0040$) creep displacement (1.04 ± 0.1 mm) compared to intact values. Following repair, step and creep displacement values (1.61 ± 0.4 mm and 1.5 ± 0.1 mm, respectively) demonstrated a restoration to intact values (1.22 ± 0.3 mm and 1.45 ± 0.1 mm, respectively; $p > 0.05$) as was indicated by a lack of statistical difference comparing between the two groups. Early viscoelastic creep response coefficients, Ψ_1 and η_1, were significantly lower for both the discectomy (Ψ_1: 663.9 ± 65.9; $p = 0.0137$ and η_1: 6.8 ± 0.9; $p = 0.0343$, respectively) and repair (Ψ_1: 445.2 ± 55.3; $p = 0.0070$ and η_1: 4.9 ± 0.9 $p = 0.0087$, respectively) groups compared to the intact testing condition. Viscoelastic coefficients reflecting late creep response, Ψ_2 and η_2, demonstrated significant increases in the annulotomy (Ψ_2: 215.6 ± 15.4; $p = 0.0011$ and η_2: 72.3 ± 5.3; $p = 0.0108$, respectively) and discectomy (Ψ_2: 254.2 ± 21.9; $p = 0.0002$ and η_2: 73.2 ± 5.2; $p = 0.0056$, respectively) groups compared to intact controls. The Ψ_2 of the repaired group (Ψ_2:197.1 ± 12.7; $p = 0.0108$) was significantly different compared to intact values whereas the long-term creep parameter η_2 was not statistically different from intact which demonstrated restoration in the repair group (η_2: 47.9 ± 2.86).

3.5. Non-crosslinked AFRPs prevent NPR herniation from IVDs

Compressive failure strength of the repaired FSUs was assessed under axial compression testing concomitant with visually assessing for AFRP attachment failure and/or ABNP herniation. Testing to failure in all cases was stopped once an average compressive stress of 4.74 ± 0.43 MPa and compressive displacement of 3.0 ± 0.21 mm was achieved. At this point, video recordings (Supplemental Video) illustrated that the vertebral endplates contacted each other and axial load was no longer applied. Macroscopic and video analysis illustrated that although outward bulging of the AFRP was noted, no failure was observed in that the AFRP did not rupture, nor did herniation/extrusion of ABNP occur.

3.6. Collagen stability of AFRPs is enchanced by crosslinking

DSC analysis illustrated T_d values of 73.61 ± 1.93 °C, 67.22 ± 0.14 °C, and 64.86 ± 0.29 °C for the native bovine AF, fresh and decellularized porcine pericardium, respectively. T_d values increased for AFRPs crosslinked with 6 mM and 30 mM EDC and 0.2% and 0.6% GLUT: 78.66 ± 0.31 °C, 86.0 ± 0.37 °C, 87.5 ± 0.26 °C and 90.28 ± 2.0 °C, respectively. Compared to native AF and pericardial tissue, these increases were significant ($p = 0.0001$ for all groups) for the EDC and GLUT treated AFRPs.

3.7. Crosslinked AFRPs resist accelerated collagenase degradation

AFRPs were subjected to accelerated collagenase digestion to assess AF resistance to the degradative environment associated IVDD (Supplemental Fig. 2). Following 1 day in digestion solution, non-crosslinked controls lost 46.3 ± 7.1% of their dry mass, while EDC

and GLUT crosslinked AFRP groups experienced statistically lower ($p = 0.0001$ for all groups) mass loss (6 mM EDC: 2.0 ± 1.0%, 30 mM EDC: 3.8 ± 1.0%, 0.2% GLUT: 1.3 ± 1.0%, and 0.6% GLUT: 2.0 ± 1.7%, respectively). Subsequently, by day 7 a statistical increase in mass loss for non-crosslinked controls (80.8 ± 4.5% average mass loss) occurred compared to day 1 values. However, mass loss did not significantly progress in the EDC or GLUT treated AFRPs compared to their respective day 1 values. After subjecting AFRPs to an enzyme solution containing a 10-fold increase in collagenase, day 14 samples demonstrated a significant increase in collagenase induced mean mass loss for EDC and GLUT samples (6 mM EDC: 10.0 ± 2.3%; $p = 0.029$, 30 mM EDC: 9.5 ± 1.9%; $p = 0.008$, 0.2% GLUT: 7.0 ± 0.8%; $p = 0.0097$, and 0.6% GLUT: 6.8 ± 1.0% $p = 0.0447$, respectively), but these values were significantly lower ($p = 0.0001$) than non-crosslinked controls (100 ± 0.0% average mass loss). Additionally, significant difference in mass loss comparing between EDC and GLUT treated AFRPs was not evident by day 14, indicating both crosslinking methods imparted similar levels of collagen protection.

3.8. AFRP tensile properties are not altered by crosslinking

Tensile testing of crosslinked 3-ply AFRPs demonstrated that crosslinking itself had minimal effects on AFRP tensile mechanical properties. EM for non-crosslinked controls (18.73 ± 1.56 MPa) was not statistically different from EDC (6 mM EDC: 16.05 ± 2.15 MPa, 30 mM EDC: 15.63 ± 2.4 MPa) or GLUT (0.2% GLUT: 14.73 ± 2.37 MPa, and 0.6% GLUT: 17.06 ± 1.11 MPa) crosslinked groups (Fig. 5A–C). Additionally, UTS of non-crosslinked controls (7.09 ± 0.48 MPa) was not statistically different from 6 to 30 mM EDC or 0.2% and 0.6% GLUT (7.83 ± 0.43 MPa, 5.71 ± 1.02 MPa, 5.85 ± 0.93 MPa, and 6.65 ± 0.55 MPa, respectively). However, tensile strain at failure (TSF) of these groups demonstrated an increasing trend, 77.71 ± 6.9%, 92.69 ± 15.81%, 101 ± 14.9%, and 92.96 ± 11.87%, respectively versus non-crosslinked controls (70.74 ± 3.21%). Additionally, all groups retained comparable mechanical properties to values reported for native human AF (EM: 19.8 MPa, UTS: 5.9 MPa, and TSF: ~65%, respectively) [34,46,50].

3.9. Crosslinked AFRPs support AF cell viability

LDH content of culture media from non-crosslinked AFRPs after 3, 6, and 12 days of culture was 21.5 ± 1.2%, 39.6 ± 3.7%, and 35.0 ± 1.1%, respectively as compared to positive death control values at each respective time point (Fig. 6B). Both 6 mM and 30 mM EDC treated AFRPs demonstrated low levels of LDH (6 mM: 26.4 ± 1.3%, 41.3 ± 1.7%, and 34.1 ± 1.4%; 30 mM: 39.2 ± 2.1%, 36.5 ± 2.3%, and 37.7 ± 1.7%, respectively) which were not significantly different from non-crosslinked controls. Additionally, non-crosslinked and EDC treated AFRPs illustrated no statistical increase in cytotoxicity between days 3, 6, and 12 within each group. Thus, indicating there was no increase in cell death with increasing time in culture. However, both 0.2% and 0.6% GLUT treated AFRPs demonstrated significantly higher ($p = 0.0001$ for all groups) cytotoxicity across each respective time point (0.2% GLUT: 159.4 ± 5.5%, 97.9 ± 2.6%, and 74.7 ± 9.3%; 0.6% GLUT: 104.5 ± 8.1%, 152.8 ± 8.2%, and 84.6 ± 3.0%, respectively) compared to non-crosslinked controls. Furthermore, high levels of cytotoxicity for GLUT samples were further validated with the relative absence of cells within histological samples (Fig. 6C) obtained at each respective time point.

3.10. AF cell infiltration is limited within crosslinked AFRPs

Cellular migration within tissue engineering scaffolds is required for tissue ingrowth and regeneration. Therefore, 3-ply AFRPs were evaluated histologically for average bAFC infiltration depth (defined as the average infiltration depth of bAFCs from the seeded ply surface) (Fig. 7). Representative sections of non-crosslinked AFRPs demonstrated an average bAFC infiltration depth of 105 ± 4.8 μm (71.1 ± 3.2% overall relative tissue thickness [RTT] by day 12), and a maximum bAFC infiltration depth (defined as the farthest bAFC distance from the seeded ply surface) of 141 μm (95.6% overall RTT). However, following EDC crosslinking bAFCs were found forming a monolayer on the outer seeded edge surfaces of the AFRP plies with minimal infiltration observed. At day 12, 6 mM EDC crosslinked AFRPs illustrated a bAFC infiltration depth of 3.62 ± 0.2 μm (1.4 ± 0.1% overall RTT) and a maximal infiltration depth of 4.7 μm (1.7% overall RTT) which was statistically lower ($p = 0.0058$) compared to non-crosslinked controls. Similarly, 30 mM EDC crosslinked AFRPs demonstrated an average bAFC infiltration depth of 14.9 ± 2.9 μm (6.8 ± 1.3% overall RTT) and a maximum infiltration depth of 35.7 μm (16.4% overall RTT), which was statistically greater ($p = 0.0089$) compared to 6 mM EDC crosslinked AFRPs, however infiltration depth was statistically lower ($p = 0.0001$) compared to non-crosslinked controls.

3.11. Sonication of crosslinked AFRPs enchances AF cell infiltration and does not detrimentally alter tensile properties

To increase cellular infiltration into the optimized 6 mM EDC crosslinked AFRPs, 3-ply samples were sonicated for various times. Sonication has been demonstrated to disrupt fibrous tissue architecture and promote cell infiltration. Representative histological sections subjected to 1-, 5-, and 10-min sonication periods illustrated an increased average bAFC infiltration depth of 149 ± 31.6 μm (27.4 ± 5.8% overall relative tissue thickness), 234.7 ± 37.8 μm (50.6 ± 8.2% overall RTT), and 98.0 ± 19.3 μm (33.4 ± 6.6% overall RTT), respectively by day 14 (Fig. 8). The maximum bAFC infiltration depth of 1-, 5-, and 10-min sonicated crosslinked AFRPs was 333.9 μm (72.0% overall relative tissue thickness), 416.3 μm (89.7% overall RTT), and 272.9 μm (93% overall RTT), respectively. Overall, histological analysis following 7 and 14 days of cell culture illustrated AFRPs subjected to 5- and 10-min sonication periods demonstrated improved cell presence on the middle ply of the AFRPs and enhanced bAFC infiltration within all plies. All sonicated testing groups demonstrated a significant increase (1- vs. 5-min: $p = 0.0058$; 1- vs 10-min: $p = 0.0009$) in maximum cell infiltration depth compared to non-sonicated controls. Additionally, AFRPs sonicated for 5-min demonstrated a significant increase ($p = 0.0001$) in maximum bAFC infiltration depth compared to a 1-min sonication period.

Based on histological results of improved bAFC infiltration, tensile testing of 6 mM EDC crosslinked 3-ply AFRPs was performed following 5- and 10-min sonication periods to evaluate the effect of sonication times on AFRP tensile mechanical properties. Following sonication, the EM for 5- and 10-min sonicated 6 mM EDC treated AFRPs (17.36 ± 1.88 MPa and 11.42 ± 1.78 MPa, respectively) were not statistically different from non-sonicated 6 mM EDC treated AFRPs (16.05 ± 2.15 MPa) (Supplemental Fig. 3). However, the EM of 10-min sonicated AFRPs was significantly lower ($p = 0.0083$) than AFRPs subjected to 5-

min sonication. Additionally, 5- and 10-min sonication periods did not significantly alter the UTS of 6 mM EDC treated AFRPs (6.07 ± 0.95 MPa and 6.38 ± 1.19 MPa, respectively) compared to non-sonicated 6 mM EDC treated AFRPs (7.83 ± 0.43 MPa). However, tensile strain at failure (TSF) tended to be lower (not statistically) for the 6 mM EDC treated AFRPs exposed to 5- and 10-min sonication periods (63.31 ± 1.77% and 74.17 ± 11.57%, respectively) versus non-sonicated 6 mM EDC treated AFRPs (77.71 ± 6.9%).

4. Discussion

To date, few biomaterials developed for AF repair have been extensively evaluated for their mechanical characteristics and ability to restore FSU kinematics. Likipanichkul et al. describe the mechanical evaluation of a cytocompatible fibrin-based injectable hydrogel for inner AF repair which demonstrated resistance to expulsion following dynamic compression and restoration of compressive stiffness following implantation into bovine FSUs [33]. More recently, the fibrin-based hydrogel was combined with a synthetic NP scaffold and a polyurethane membrane sutured to the outer AF to repair FSUs. Biomechanical evaluations of the repaired FSUs commonly demonstrated NP scaffold herniation/extrusion from the IVDs when physiological loading was applied [35]. In this investigation, we have demonstrated an in-depth mechanical characterization of a collagen-based, multi-laminate angle-ply AF repair patch (AFRP) biomaterial that illustrated its ability to mimic the static and dynamic biomechanical characteristics of the native human AF. Additionally, a second major finding of this study demonstrated that the use of the AFRP could prevent herniation of an NPR and aids in the restoration of axial kinematics of FSUs following aggressive discectomy and application of physiologic loading. A third major finding of this study confirmed that chemical crosslinking of AFRPs rendered them resistant to accelerated collagenase degradation without detrimentally impacting AFRP tensile mechanical properties or AF cell viability.

The AF is composed of an angle-ply architecture which exhibits unique material properties which are dependent on orientation (axial, circumferential, or radial), hierarchical structure (single lamellae or multi-laminate), and anatomic location (anterior, posterior, inner, or outer AF) [34,51]. The primary role of the AF is to mechanically confine the NP by providing resistance to IDP through the generation of tensile hoop stresses, while resisting tensile stretching and torsional rotations. Human lumbar IVDs can experience axial compressive loads ranging from 340 to 1200 N during activities of daily living and up to 2350 N during strenuous activities which can result in the generation of IDPs ranging from 0.1 to 2.3 MPa that must be endured by the AF [52–54]. The tensile material properties of the AF, including its UTS (3.8 MPa), EM (12–24 MPa), and TSF (~65% in fully flexed position) allow for it to bear such stresses [37,41,46], in addition to allowing the AF to withstand varying applied strain rates arising from complex intradiscal deformations and strain patterns [3]. Considering this, an effective AF repair device must recapitulate these material parameters to function and survive within the mechanical environment of the IVD.

Accordingly, AFRPs were evaluated for several mechanical characteristics. First, we evaluated the ability of AFRPs to absorb energy and resist impact loading as sudden variations in applied force with respect to time (i.e. ‘jerk’ or ‘force-jerk’ loading) can occur

when missing a step for falling on your buttocks [55–57], which results in increased IDPs [58,59], and can lead to AF rupture [60]. The AFRP demonstrated the ability to withstand up to 3 g-force (equivalent to a rollercoaster ride) prior to failure. Second, considering that lumbar IVDs undergo millions of loading cycles over the life of the patient, AFRPs were evaluated for their tensile fatigue strength. Previous reports by others have demonstrated that human lumbar AF promptly fails following the application of cyclic tensile stress amplitudes ranging from 2.5 to 3 MPa, whereas application of moderate amplitudes (reminiscent of those experienced during activities of daily living) result in years of functionality [46]. Under similar test conditions, the AFRP illustrated a S-N curve profile comparable to full-thickness human lumbar AF when subjected to low stress amplitudes (1.5–2 MPa); however, AFRPs demonstrated enhanced durability compared to native AF tissue tested at moderate and high stress amplitude ranges (2–3 MPa). Finally, the attachment strength of the AFRP to IVDs were investigated as many clinical studies have demonstrated this to be an ‘Achilles heel’ of current AF repair devices causing them to fail at stresses approaching 1.5 MPa [20,21,61–65]. Herein, we utilized a simple suturing technique using 4–0 FiberWire suture. Burst strength testing of the AFRP attachment to the IVD demonstrate that the suturing technique employed can withstand physiologically relevant stresses without failure. Although suturing in the confined space of the posterolateral spine using minimally invasive spine surgery techniques can be challenging, nervous tissue can be gently retracted and suture can be placed in the four corners of the AFRP prior to introducing it down a tubular retractor.

The primary function of the IVD is to allow for flexibility of the spine and thus together, the healthy NP and AF help maintain normal spinal kinematics. Two primary kinematic parameters are often used to define spinal motion: 1) NZ (i.e. the absolute measure of joint laxity around the neutral position demonstrating minimal internal resistance), and 2) RoM (i.e. the entire range of the physiological spinal segment motion). Reported NZ and RoM values for healthy human lumbar spine segments are 10.4° and 7.6°, 1.5° and 3.8°, 1.6° and 6.6°, and 0.7° and 2.4° in flexion, extension, lateral bending, and torsion, respectively [66]. During IVDD these parameters often change [66,67]. The primary goal of NPR and AF repair devices is to restore normal spinal kinematics to healthy (intact) values. In general, when used together our ABNP and AFRP were able to restore axial FSU kinematics following repair.

Creep displacement of the IVD is thought to be dominated by the NP in the short-term, and by the AF in the long-term [36]. This was supported by the testing herein of annulotomized FSUs which resulted in significant changes in the long-term creep parameters. In addition, FSUs that subsequently underwent aggressive nucleotomy demonstrated persistent long-term changes in creep parameters in addition to imparting detrimental effects in the short-term creep parameters. Repair of the IVD with the ABNP and AFRP helped restore these values. However, the short-term creep response remained significantly lower in the repaired group as compared to intact, likely due to the swollen and porous nature of the ABNP leading to increase fluid diffusivity and a reduced capacity to resist compressive loading. Cyclic testing data demonstrated statistical increases in RoM following discectomy and subsequent restoration towards intact values following repair with the AFRP and ABNP biomaterials. There was no significant difference observed in the constant slow ramp

compressive stiffness comparing intact and repaired FSUs, however compressive stiffness of injured IVDs was significantly lower compared to the intact condition.

Subsequent to kinematic testing, compression to failure testing was used to evaluate AFRP repair strength under extreme axial loading conditions [52,53]. The strength of attachment of the AFRP exceeded values obtained during biaxial ball-burst testing. It was also noted that no ABNP material extruded but that the vertebral end-plates eventually contacted each other. This is likely explained by two potential phenomena; 1) the nucleotomy space may have not been completely filled with ABNP and/or 2) when the ABNP was compressed at supraphysiological loads (>2.5 MPa) the water within the ABNP was driven out effectively depressurizing the material thus allowing the end-plates to make contact.

Disc degeneration is best defined as an aberrant cell-mediated process that results in ECM degradation eventuating in the structural demise of the IVD. Increasing grades of IVDD have been positively correlated with increasing concentrations of proteases. More specifically, mean concentrations of MMP-1 (collagenases type I) have been shown to increase with increasing grades of IVDD (grade III: 133 pg/ml, grade IV: 279 pg/ml, grade V: 319 pg/ml) [40]. Therefore, any ECM-based biomaterial placed in this caustic environment must resist accelerated degeneration so that it can maintain its mechanical integrity and function. To prevent collagen degradation, AFRPs were crosslinked using well-established chemistries and were evaluated for accelerated mass loss following incubation in collagenase concentrations that were 1000–10,000 times the concentrations typically found in the degenerative IVD. Minimal degradation was observed in EDC and GLUT crosslinked AFRPs that may be advantageous allowing for prolonged mechanical function of the biomaterial and eventual tissue remodeling and regeneration. The tensile mechanical properties of AFRPs did not change significantly following crosslinking; this was likely due to the testing rate used to assess the AFRPs. Jang et al. has previously demonstrated that when pericardium tissue is tested under high tensile strain rates (>100 mm/min; similar to testing rates of native AF tissue) the viscoelastic nature of the tissue predominates the effect of different crosslinking chemistries on its mechanical properties [68].

Tissue remodeling and regeneration are in large part influenced by cytotoxicity of the biomaterial and the ability of cells to infiltrate into the AFRP. Previous studies by others have demonstrated the cytocompatibility of EDC when used as a collagen crosslinker [36]. Conversely, while GLUT crosslinking has been shown to effectively stabilize tissue engineered scaffolds, it significantly reduces cell viability likely due to the toxicity of unreacted side-groups [69,70]. Herein, we examined the effects of EDC and GLUT crosslinking chemistries on AF cell cytotoxicity and infiltration into the AFRP. Non-statistical differences were observed comparing between non-crosslinked and EDC treated AFRPs demonstrating their cytocompatibility. However, AF cell infiltration was significantly hampered as has been previously observed by others [69], likely due to the high density of ‘zero-length’ crosslinks created between collagen molecules. Thus, ultrasonication; a procedure previously demonstrated to increase porosity and thus cell infiltration depth, was used to mechanically disrupt the AFRPs [71]. Subsequent mechanical testing of AFRPs demonstrated that the tensile properties of the biomaterial were not detrimentally altered following 5-min sonication periods, yet bAFC infiltration depth was

statistically increased. Together, these results suggest the AFRP is cytocompatible and will allow endogenous or exogenous cells to infiltrate and potentially remodel the AFRP.

5. Limitations

As with any study, the authors acknowledge some limitations within this study. First, fatigue testing was only run to a maximum of 10,000 cycles despite the spine undergoing millions of cycles over the lifetime of an individual. However, there are only a limited number of daily activities (i.e. those involving bending at the waist) which would create the stress amplitudes evaluated herein. Therefore, the AF may only be subjected to these stresses a few times per day and thus achieving 10,000 cycles of fatigue would represent years to a decade of *in vivo* use [46]. The authors also recognize that the full-thickness human AF constitutes a gradient of ECM components and material properties while the AFRP described herein anatomically represents only the outer AF. Despite this, our results demonstrate that the 3-ply AFRP has the tensile strength typically observed for a full-thickness segments of human posterolateral AF [46]. Moreover, the authors recognize that inclusion of an additional testing group (i.e. repaired annulotomy) within the kinematic study may have more clearly delineated the exact contribution of the AFRP and ABNP to FSU kinematics; however, we did not want to induce excessive damage to the native AF via repeated attachment and detachment of the AFRP following annulotomy and discectomy. It should also be noted that the AFRPs were sterilized using 0.1% peracetic acid, however further study is warranted to evaluate other commonly used medical device sterilization techniques and their effect on AFRP mechanical properties and cytocompatibility. Finally, the authors also recognize that the laboratory based mechanical testing performed herein do not reflect the potential changes in AFRP or suture strength or accumulation of damage over time when implanted *in vivo*.

6. Conclusion

In conclusion, the AFRP has demonstrated its mechanical appropriateness for implantation into the mechanically demanding environment of the spine while illustrating its biologic functionality supporting IVD cell activity. Utilization of this biomaterial may allow for the implementation of interventional strategies thereby potentially improving clinical outcomes for a significant number patients suffering from IVD degeneration and/or herniation. On-going work includes evaluating the ability of the AFRP and ABNP to support stem cell differentiation and tissue regeneration *in vitro* and their ability to mitigate IVD degeneration in a large animal model.

Supplementary Material

Refer to Web version on PubMed Central for supplementary material.

Acknowledgments

Research support for the Ortho-X lab has been provided in part by the National Institute of General Medical Sciences of the National Institutes of Health (award number: 5P20GM103444-07) and departmental start-up funds. R. Borem is supported by the National Science Foundation Graduate Research Fellowship (grant number:

2011382). Additionally, we would like to thank Mr. Alan Marionneaux for his assistance in analyzing kinematic creep data.

Appendix A. Supplementary data

Supplementary data associated with this article can be found, in the online version, at http://dx.doi.org/10.1016/j.actbio.2017.06.006.

References

1. Urban JPG, Roberts S. Degeneration of the intervertebral disc. Arthritis Res Ther. 2003; 5:120. http://dx.doi.org/10.1186/ar629. [PubMed: 12723977]
2. McNally M, Adams DS. Internal intervertebral disc mechanics as revealed by stress profilometry. Spine. 1992; 17:66–73. 1976. http://dx.doi.org/10.1097/00007632-199201000-00011. [PubMed: 1536017]
3. Stokes I. Surface strain on human intervertebral discs. J Orthop Res. 1987; 5:348–355. http://dx.doi.org/10.1002/jor.1100050306. [PubMed: 3625358]
4. Praemer D, Furner A, Rice S. Musculoskeletal conditions in the United States. Am Acad Orthop Surg. 1999
5. Freemont TJ, LeMaitre C, Watkins A, Hoyland JA. Degeneration of intervertebral discs: current understanding of cellular and molecular events, and implications for novel therapies. Expert Rev Mol Med. 2001; 3:1–10. http://dx.doi.org/10.1017/S1462399401002885.
6. Adams MA, Freeman BJ, Morrison HP, Nelson IW, Dolan P. Mechanical initiation of intervertebral disc degeneration. Spine. 2000; 25:1625–1636. http://dx.doi.org/10.1097/00007632-200007010-00005. [PubMed: 10870137]
7. Mannion AF, Adams MA, Dolan P. Sudden and unexpected loading generates high forces on the lumbar spine. Spine. 2000; 25:842–852. http://dx.doi.org/10.1097/00007632-200004010-00013. [PubMed: 10751296]
8. Horner HA, Urban JP. Volvo award winner in basic science studies: effect of nutrient supply on the viability of cells from the nucleus pulposus of the intervertebral disc. Spine. 2001; 26:2543–2549. http://dx.doi.org/10.1097/00007632-200112010-00006. [PubMed: 11725234]
9. Brown P, Malinin MD, Davis TI. A roentgenographic evaluation of frozen allografts versus autografts in anterior cervical spine fusions. Clin Orthop Relat Res. 1976; 119:231–236.
10. Bibby SRS, Urban JPG. Effect of nutrient deprivation on the viability of intervertebral disc cells. Eur Spine J. 2004; 13:695–701. http://dx.doi.org/10.1007/s00586-003-0616-x. [PubMed: 15048560]
11. Yang X, Li X. Nucleus pulposus tissue engineering: a brief review. Eur Spine J. 2009; 18:1564–1572. http://dx.doi.org/10.1007/s00586-009-1092-8. [PubMed: 19603198]
12. Taylor D, Deyo VM, Cherkin RA. Low back pain hospitalization. Recent United States trends and regional variations. Spine. 1994; 19:1207–1212. [PubMed: 8073311]
13. Wipf JE, Deyo RA. Low back pain. Med Clin North Am. 1995; 79:231–246. [PubMed: 7877388]
14. Hart D, Deyo LG, Cherkin RA. Physician office visits for low back pain: frequency, clinical evaluation, and treatment patterns from a U.S. national survey. Spine. 1995; 20:11–19. [PubMed: 7709270]
15. Martin BI, Deyo RA, Mirza SK, Turner JA, Comstock BA, Hollingworth W, Sullivan SD. Expenditures and health status among adults with back and neck problems. JAMA. 2008; 299:656–664. http://dx.doi.org/10.1001/jama.299.6.656. [PubMed: 18270354]
16. Sharifi, S., Bulstra, SK., Grijpma, DW., Kuijer, R. Treatment of the degenerated intervertebral disc; closure, repair and regeneration of the annulus fibrosus. J Tissue Eng Regen Med. 2015. http://dx.doi.org/10.1002/term.1866
17. Khan SN, Stirling AJ. Controversial topics in surgery: degenerative disc disease: disc replacement. Ann R Coll Surg Engl. 2007; 89:6–11. http://dx.doi.org/10.1308/003588407X160792.

18. Mercuri JJ, Gill SS, Simionescu DT. Novel tissue-derived biomimetic scaffold for regenerating the human nucleus pulposus. J Biomed Mater Res Part A. 2011; 96 A:422–435. http://dx.doi.org/10.1002/jbm.a.33001.
19. Fernandez, C., Marionneaux, A., Gill, S., Mercuri, J. Biomimetic nucleus pulposus scaffold created from bovine caudal intervertebral disc tissue utilizing an optimal decellularization procedure. J Biomed Mater Res Part A. 2016. http://dx.doi.org/10.1002/jbm.a.35858
20. Bailey A, Araghi A, Blumenthal S, Huffmon GV. Prospective, Multicenter, Randomized, Controlled Study of Anular Repair in Lumbar Discectomy and the Anular Repair Clinical Study Group. Randomized Trial Spine. 38:1161–1169. n.d. DOI: 10.1097/BRS.0b013e31828b2e2f
21. Lequin MB, Barth M, Thomė C, Bouma GJ. Primary limited lumbar discectomy with an annulus closure device: one-year clinical and radiographic results from a prospective, multi-center study. Korean J Spine. 2012; 9:340–347. [PubMed: 25983843]
22. Hu G, Jaglal RW, Axcell S, Anderson T. A population-based study of reoperations after back surgery. Spine. 1997; 22:2265–2270. [PubMed: 9346147]
23. Atlas D, Keller SJ, Wu RB, Deyo YA, Singer RA. Long-term outcomes of surgical and nonsurgical management of sciatica to a lumbar herniation: 10 year results from the maine lumbar spine study. Spine. 2005; 30(30):927–935. [PubMed: 15834338]
24. Medical M. Global Orthopedic Device Market (Hip, Knee, Spine, Extremities and Trauma Devices). Kalorama Inf. 2015
25. Insight M. US Markets for Nonfusion Spinal Technologies and Disc Diagnostic Devices Report #A317. 2013
26. Wilke HJ, Widmann L, Graf N, Heuer F. Can herniation be prevented? establishment of a herniation model and experiments with an annulus reconstruction implant. Spine J. 2011; 11:S148–S149. http://dx.doi.org/10.1016/j.spinee.2011.08.358.
27. Olmarker K. Neovascularization and Neoinnervation of Subcutaneously Placed Nucleus Pulposus and the Inhibitory Effects of Certain Drugs. Spine. 30:1501–1504. n.d.
28. Nygaard OP, Mellgren SI, Osterud B. The inflammatory properties of contained and noncontained lumbar disc herniation. Spine. 1997; 22:2484–2488. http://dx.doi.org/10.1097/00007632-199711010-00004. [PubMed: 9383853]
29. Coppes MH, Marani E, Thomeer RT, Groen GJ. Innervation of “painful” lumbar discs. Spine. 1997; 22 2342-9-50.
30. Pirvu T, Blanquer SBG, Benneker LM, Grijpma DW, Richards RG, Alini M, Eglin D, Grad S, Li Z. A combined biomaterial and cellular approach for annulus fibrosus rupture repair. Biomaterials. 2015; 42:11–19. http://dx.doi.org/10.1016/j.biomaterials.2014.11.049. [PubMed: 25542789]
31. Nerurkar, NL., Elliott, DM., Mauck, RL. Mechanics of oriented electrospun nanofibrous scaffolds for annulus fibrosus tissue engineering. J Orthop Res. 2007. http://dx.doi.org/10.1002/jor.20384
32. Chang G, Kim HJ, Vunjak-Novakovic G, Kaplan DL, Kandel R. Enhancing annulus fibrosus tissue formation in porous silk scaffolds. J Biomed Mater Res Part A. 2010; 92:43–51. http://dx.doi.org/10.1002/jbm.a.32326.
33. Likhitpanichkul J, Dreischarf M, Illien-Junger M, Walter S, Nukaga B, Long T, Sakai R, Hecht D, Iatridis A. Fibrin-genipin adhesive hydrogel for annulus fibrosus repair: performance evaluation with large animal organ culture, in situ biomechanics, and in vivo degradation tests. Eur Cells Mater. 2014; 28:25–38.
34. Long RG, Torre OM, Hom WW, Assael DJ, Iatridis JC. Design Requirements for Annulus Fibrosus Repair: Review of Forces, Displacements, and Material Properties of the Intervertebral Disk and a Summary of Candidate Hydrogels for Repair. n.d.
35. Long, RG., Bürki, A., Zysset, P., Eglin, D., Grijpma, DW., Blanquer, SBG., Hecht, AC., Iatridis, JC. Mechanical restoration and failure analyses of a hydrogel and scaffold composite strategy for annulus fibrosus repair. Acta Biomater. 2016. http://dx.doi.org/10.1016/j.actbio.2015.11.015
36. Johannessen W, Cloyd JM, O’Connell GD, Vresilovic EJ, Elliott DM. Transendplate nucleotomy increases deformation and creep response in axial loading. Ann Biomed Eng. 2006; 34:687–696. http://dx.doi.org/10.1007/s10439-005-9070-8. [PubMed: 16482409]

37. O'Connell, GD., Sen, S., Elliott, DM. Human annulus fibrosus material properties from biaxial testing and constitutive modeling are altered with degeneration. Biomech Model Mechanobiol. 2012. http://dx.doi.org/10.1007/s10237-011-0328-9
38. Urban JPG, Roberts S, Ralphs JR. The nucleus of the intervertebral disc from development to degeneration. Am Zool. 2000; 40:53–61. http://dx.doi.org/10.1668/0003-1569(2000)040[0053:TNOTID]2.0.CO;2.
39. Genevay S, Finckh A, Mezin F, Tessitore E, Guerne PA. Influence of cytokine inhibitors on concentration and activity of MMP-1 and MMP-3 in disc herniation. Arthritis Res Ther. 2009; 11 http://dx.doi.org/10.1186/ar2858.
40. Mern, DS., Fontana, J., Beierfuß, A., Thomé, C., Hegewald, AA. A combinatorial relative mass value evaluation of endogenous bioactive proteins in three-dimensional cultured nucleus pulposus cells of herniated intervertebral discs: identification of potential target proteins for gene therapeutic approaches. PLoS One. 2013. http://dx.doi.org/10.1371/journal.pone.0081467
41. Iatridis, JC., Nicoll, SB., Michalek, AJ., Walter, BA., Gupta, MS. Role of biomechanics in intervertebral disc degeneration and regenerative therapies: what needs repairing in the disc and what are promising biomaterials for its repair?. Spine J. 2013. http://dx.doi.org/10.1016/j.spinee.2012.12.002
42. McGuire, R., Borem, R., Mercuri, J. The fabrication and characterization of a multi-laminate, angle-ply collagen patch for annulus fibrosus repair. J Tissue Eng Regen Med. 2016. http://dx.doi.org/10.1002/term.2250
43. Perie DS, Maclean JJ, Owen JP, Iatridis JC. Correlating material properties with tissue composition in enzymatically digested bovine annulus fibrosus and nucleus pulposus tissue. Ann Biomed Eng. 2006; 34:769–777. [PubMed: 16598654]
44. Freytes DO, Rundell AE, Vande Geest J, Vorp DA, Webster TJ, Badylak SF. Analytically derived material properties of multilaminated extracellular matrix devices using the ball-burst test. Biomaterials. 2005; 26:5518–5531. http://dx.doi.org/10.1016/j.biomaterials.2005.01.070. [PubMed: 15860208]
45. Crapo, PM., Gilbert, TW., Badylak, SF. An overview of tissue and whole organ decellularization processes. Biomaterials. 2011. http://dx.doi.org/10.1016/j.biomaterials.2011.01.057
46. Green TP, Adams MA, Dolan P. Tensile properties of the annulus fibrosus II. Ultimate tensile strength and fatigue life. Eur Spine J. 1993; 2:209–214. [PubMed: 20058407]
47. Elliott DM, Yerramalli CS, Beckstein JC, Boxberger JI, Johannessen W, Vresilovic EJ. The effect of relative needle diameter in puncture and sham injection animal models of degeneration. Spine. 2008; 33:588–596. http://dx.doi.org/10.1097/BRS.0b013e318166e0a2. [PubMed: 18344851]
48. Mercuri JJ, Lovekamp JJ, Simionescu DT, Vyavahare NR. Glycosaminoglycan-targeted fixation for improved bioprosthetic heart valve stabilization. Biomaterials. 2007; 28:496–503. http://dx.doi.org/10.1016/j.biomaterials.2006.09.005. [PubMed: 17030363]
49. Tam, H., Zhang, W., Feaver, KR., Parchment, N., Sacks, MS., Vyavahare, N. A novel crosslinking method for improved tear resistance andbiocompatibility of tissue based biomaterials. Biomaterials. 2015. http://dx.doi.org/10.1016/j.biomaterials.2015.07.011
50. O'Connell GD, Sen S, Elliott DM. Human annulus fibrosus material properties from biaxial testing and constitutive modeling are altered with degeneration. Biomech Model Mechanobiol. 2012; 11:493–503. http://dx.doi.org/10.1007/s10237-011-0328-9. [PubMed: 21748426]
51. Ducheyne, K., Healy, P. Comprehensive Biomaterials. Elsevier Science; 2011.
52. Patwardhan AG, Carandang G, Ghanayem AJ, Havey RM, Cunningham B, Voronov LI, Phillips FM. Compressive preload improves the stability of anterior lumbar interbody fusion cage constructs. J Bone Joint Surg Am. 2003; 85:1749–1756. [PubMed: 12954834]
53. Schultz A, Andersson G, Ortengren R, Haderspeckt K, Nachemson A. Loads on the lumbar spine validation of a biomechanical analysis by measurements of intradiscal pressures and myoelectric signals. J Bone Joint Surg Am. 1982; 64:713–720. [PubMed: 7085696]
54. Wilke H, Neef P, Caimi M, Hoogland T, Claes LE. New in vivo measurements of pressures in the intervertebral disc in daily life. Spine. 1999; 24:755–762. 1976. [PubMed: 10222525]
55. Gatt J, Hosea CJ, Palumbo TM, Zawadsky RC. Impact loading of the lumbar spine during football blocking. AM J Sport Med. 1997; 25:317–321.

56. Schafer, R., editor. Clinical Biomechanics: Musculoskeletal Actions and Reactions. 2nd. 1987.
57. van Loon R, Huyghe JM, Wijlaars MW, Baaijens FPT. 3D FE implementation of an incompressible quadriphasic mixture model. Int J Numer Methods Eng. 2003; 57:1243–1258. http://dx.doi.org/10.1002/nme.723.
58. Mustafy T, El-Rich M, Mesfar W, Moglo K. Investigation of impact loading rate effects on the ligamentous cervical spinal load-partitioning using finite element model of functional spinal unit C2–C3. J Biomech. 2014; 47:2891–2903. http://dx.doi.org/10.1016/j.jbiomech.2014.07.016. [PubMed: 25129167]
59. Mustafy T, Moglo K, Adeeb S, El-Rich M. Injury mechanisms of the ligamentous cervical C2–C3 functional spinal unit to complex loading modes: finite element study. J Mech Behav Biomed Mater. 2016; 53:384–396. http://dx.doi.org/10.1016/j.jmbbm.2015.08.042. [PubMed: 26409229]
60. Iencean SM. Lumbar intervertebral disc herniation following experimental intradiscal pressure increase. Acta Neurochir (Wien). 2000; 142:669–676. http://dx.doi.org/10.1007/s007010070111. [PubMed: 10949442]
61. Guterl CC, See EY, Blanquer SBG, Pandit A, Ferguson SJ, Benneker LM, Grijpma DW, Sakai D, Eglin D, Alini M, Iatridis JC, Grad S. Challenges and strategies in the repair of ruptured annulus fibrosus. Eur Cell Mater. 2013; 25:1–21. http://dx.doi.org/10.1016/j.jsbmb.2011.07.002.Identification. [PubMed: 23283636]
62. Bartlett A, Wales L, Houfburg R, Durfee WK, Griffith SL, Bentley I. Optimizing the effectiveness of a mechanical suture-based anulus fibrosus repair construct in an acute failure laboratory simulation. J Spinal Disord Tech. 2012; 26:1. http://dx.doi.org/10.1097/BSD.0b013e31824c8224.
63. FDA. Maude Database. 2016
64. Bron, JL., Van Der Veen, AJ., Helder, MN., Van Royen, BJ., Smit, TH. Biomechanical and in vivo evaluation of experimental closure devices of the annulus fibrosus designed for a goat nucleus replacement model. Eur Spine J. 2010. http://dx.doi.org/10.1007/s00586-010-1384-z
65. Ahlgren BD, Lui W, Herkowitz HN, Panjabi MM, Guiboux JP. Effect of anular repair on the healing strength of the intervertebral disc: a sheep model. Spine. 2000; 25:2165–2170. http://dx.doi.org/10.1097/00007632-200009010-00004. [PubMed: 10973397]
66. Panjabi MM. The stabilizing system of the spine. Part II. Neutral zone and instability hypothesis. J Spinal Disord. 1992; 5:390–396. http://dx.doi.org/10.1097/00002517-199212000-00002. discussion 397. [PubMed: 1490035]
67. McGregor AH, Cattermole HR, Hughes SP. Spinal motion in lumbar degenerative disc disease. J Bone Jt Surg Br. 1998; 80:1009–1013.
68. Jang W, Choi S, Kim SH, Yoon E, Lim HG, Kim YJ. A comparative study on mechanical and biochemical properties of bovine pericardium after single or double crosslinking treatment. Korean Circ J. 2012; 42:154–163. http://dx.doi.org/10.4070/kcj.2012.42.3.154. [PubMed: 22493610]
69. Haugh MG, Murphy CM, Mckiernan RC, Altenbuchner C, 'brien FJO. Crosslinking and mechanical properties significantly influence cell attachment, proliferation, and migration within collagen glycosaminoglycan scaffolds. Tissue Eng Part A. 2011; 17:1201–1208. http://dx.doi.org/10.1089/ten.TEA.2010.0590. [PubMed: 21155630]
70. Lee CR, Grodzinsky AJ, Spector M. The effects of cross-linking of collagen-glycosaminoglycan scaffolds on compressive stiffness, chondrocyte-mediated contraction, proliferation and biosynthesis. Biomaterials. 2001; 22:3145–3154. http://dx.doi.org/10.1016/S0142-9612(01)00067-9. [PubMed: 11603587]
71. Burden DW. Guide to the Homogenization of Biological Samples. Random Prim. 2008:1–14.

Statement of Significance

The quality of life for millions of individuals globally is detrimentally impacted by IVD degeneration and herniation. These pathologies often result in the structural demise of IVD tissue, particularly the annulus fibrosus (AF). Biomaterials developed for AF repair have yet to demonstrate the mechanical strength and durability required for utilization in the spine. Herein, we demonstrate the development of an angle-ply AF repair patch (AFRP) that can resist the application of physiologically relevant stresses without failure and which contributes to the restoration of functional spinal unit axial kinematics following repair. Furthermore, we show that this biomaterial can resist accelerated degradation in a simulated degenerate environment and supports AF cell viability.

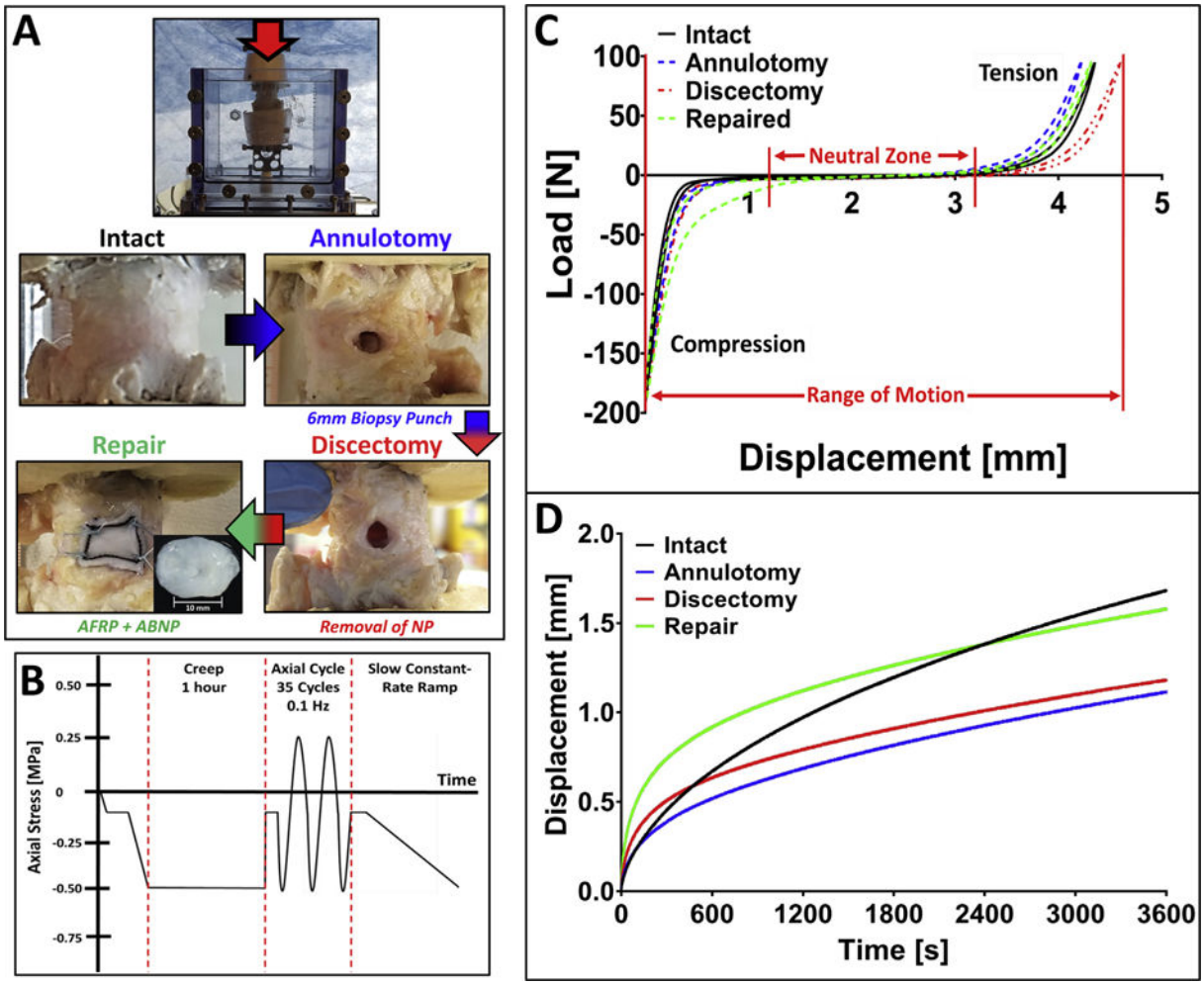

Fig. 1.

Study design for *in vitro* kinematic testing using AFRP and ABNP repair biomaterials. A) Representative images of assigned testing groups and schematic of preparation for kinematic testing of bovine caudal functional spinal units (FSUs). B) Loading scheme for FSU testing depicting creep, axial cyclic tension-compression, and slow constant-rate ramp tests. C) Representative axial force-displacement curve from axial tension-compression loading and its post-test analysis. D) Representative creep displacement curves from a single FSU. (Methods used to generate data within this figure are described in section 2.4).

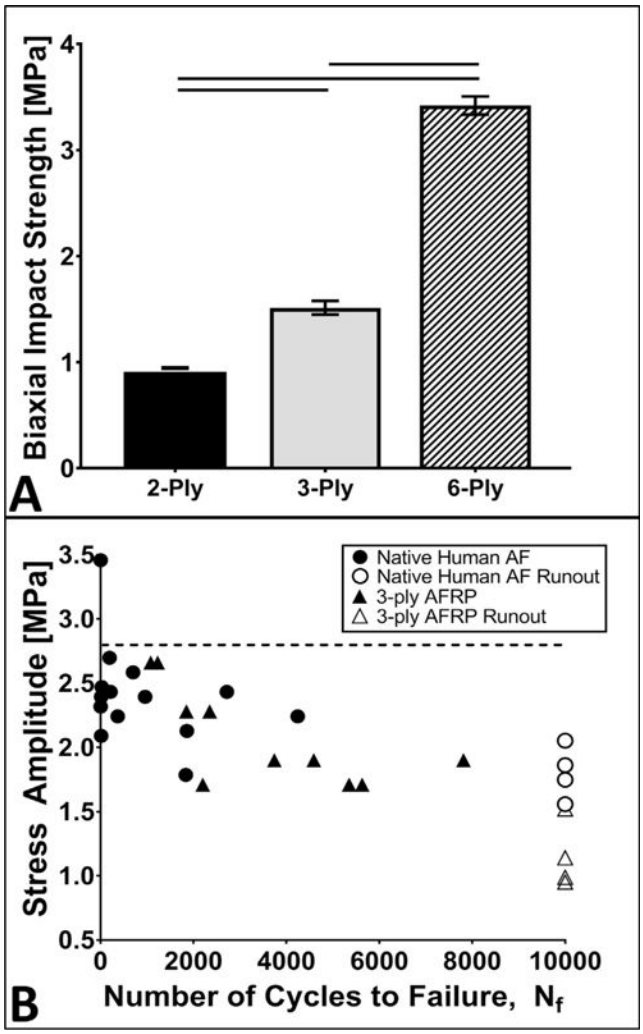

Fig. 2.

Biomechanical evaluations of non-crosslinked multi-laminate AFRPs subjected to biaxial impact burst and tensile fatigue. A) Representative graph of the average maximum calculated impact burst strength withstood by 2-, 3-, and 6-ply AFRPs. Solid lines connecting different groups on graph indicate a significant difference ($p < 0.05$). B) S-N curve illustrating the fatigue strength of 3-ply AFRPs, in comparison of native human *AF* (Dotted horizontal line indicates 70% UTS [46] of measured human *AF*. Open diamonds and triangles indicate specimens with no mechanical failure observed (i.e. run-out to 10,000 cycles). (Methods used to generate data within this figure are described in sections 2.3.1 and 2.3.2).

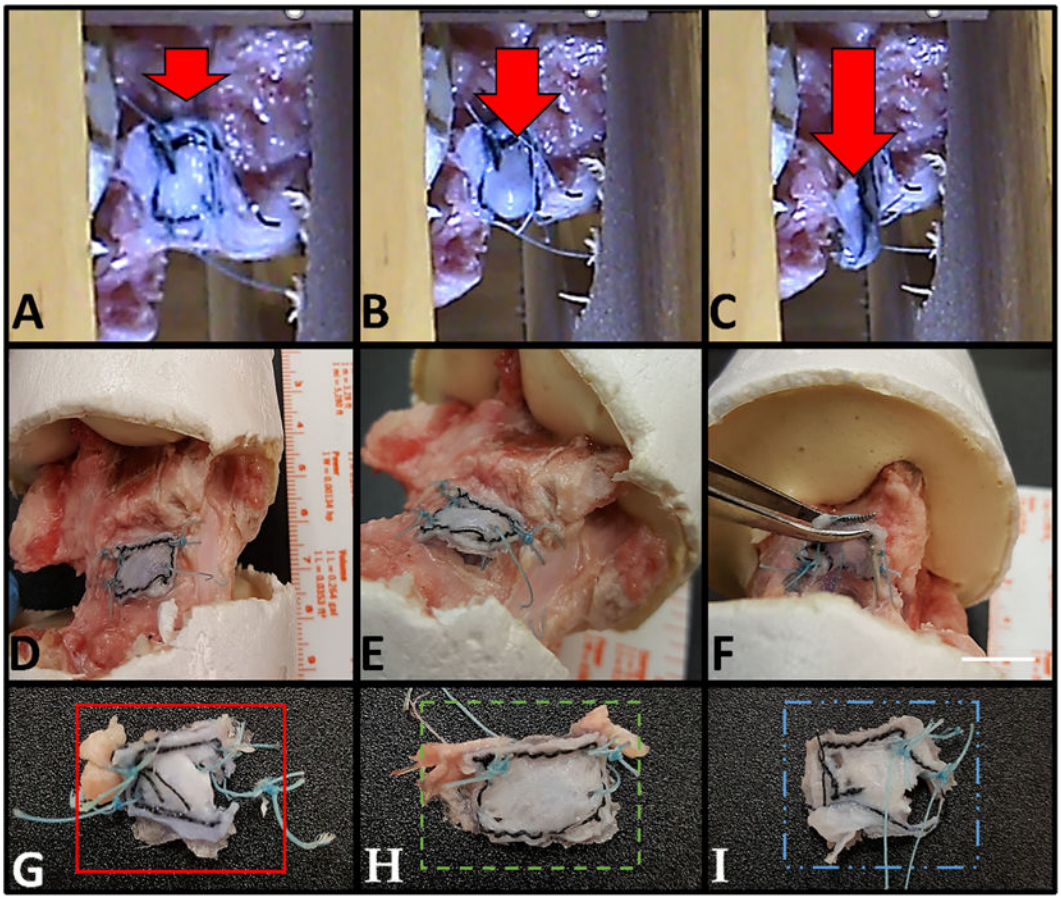

Fig. 3.

Strength of non-crosslinked AFRP attachment to IVDs. A–C) Representative images of one test specimen illustrating the eventual burst of a 6 mm stainless steel ball through an AFRP (Arrow represents direction of force applied by the ball and rod against the AFRP). D-F) Evaluation of failure mechanism prior to removal of the AFRP (Scale bar = 10 mm). G-I) AFRPs illustrating representative failure modes including; G) AFRP rupture, H) failure by suture break, and I) combined failure modes of suture break and AFRP rupture. (Methods used to generate data within this figure are described in section 2.3.3).

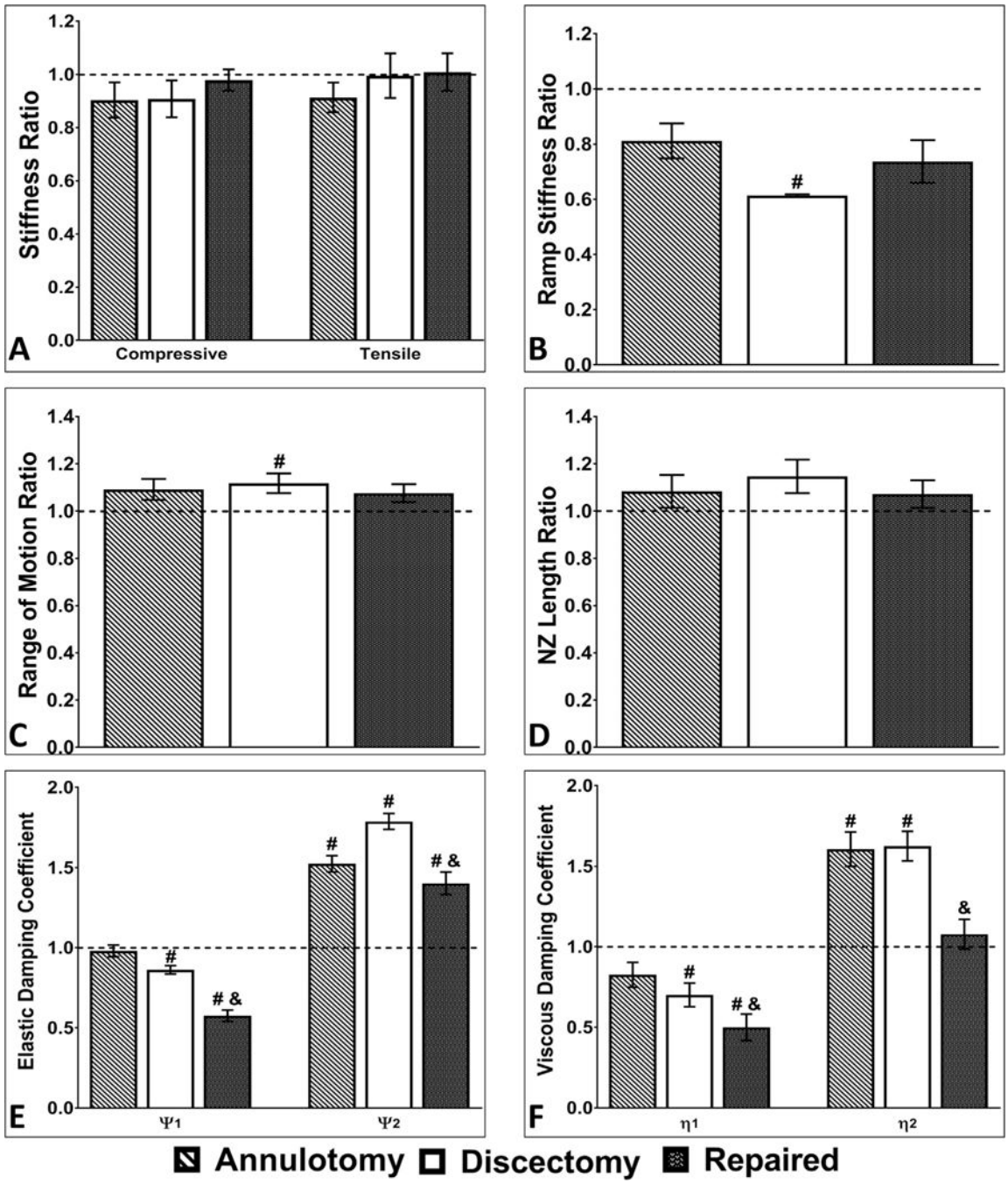

Fig. 4.

Kinematic testing results normalized to intact controls. Comparison between groups for A) compressive stiffness and tensile stiffness, B) slow constant-rate slow ramp stiffness C) axial range of motion, D) neutral zone length, and creep parameters E) elastic damping coefficients and F) viscous damping coefficients (i.e. normalized to the intact IVD (dotted black line at y = 1) for each test). Axial biomechanical parameters were partially or completely restored to Intact levels for the AFRP + ABNP repair groups. # and & on graph

indicates a significant difference ($p < 0.05$) compared to the intact or discectomy groups, respectively. (Methods used to generate data within this figure are described in section 2.4).

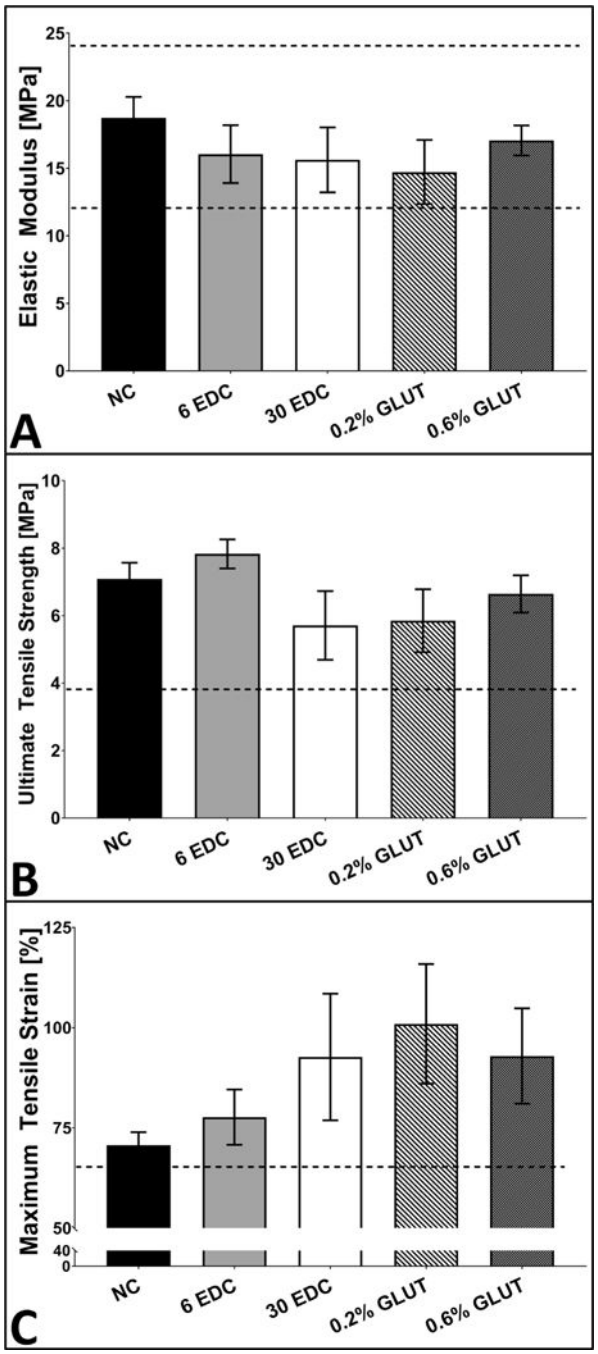

Fig. 5.

Tensile testing of crosslinked AFRPs compared to native human AF lamellae. A-C) Representative graphs illustrating mean elastic modulus (EM), ultimate tensile strength (UTS), and tensile strain at failure (TSF) for crosslinked AFRPs. (Dotted horizontal line indicates human AF tensile properties reported in literature) [34,46,50]. (Methods used to generate data within this figure are described in section 2.5.4).

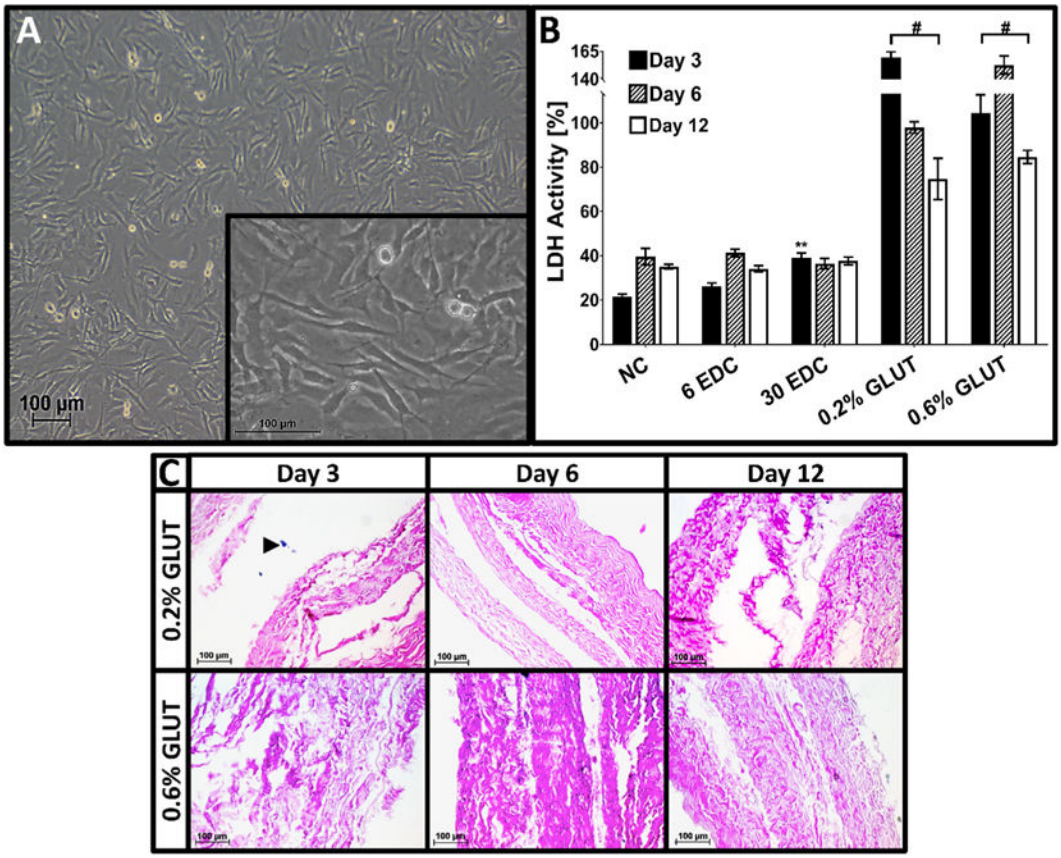

Fig. 6.

Cytotoxicity of crosslinked AFRPS. A) Representative image of bovine AF cells (bAFCs) (P2) (100×) harvested and isolated from skeletally mature bovine caudal IVDs (Insert: Representative image of AF cell fibroblast-like phenotype (400×)). B) Graph illustrating percent lactate dehydrogenase (LDH) produced by bAFC seeded 3-ply AFRPs following seeding and culture of 3, 6, and 12 days relative to a positive cell death control (i.e. bAFC seeded 3-ply AFRPs subjected to snap freezing with liquid nitrogen to induce 100% cell death). Solid lines with (#) connecting different study groups on graphs indicate a significant difference ($p < 0.05$) from non-crosslinked controls. C) Representative H&E images (200×) of 0.2% and 0.6% GLUT crosslinked AFRPs illustrating minimal to no cell presence at respective time points. (Black arrow head indicates cell nuclei). (Methods used to generate data within this figure are described in section 2.6.3).

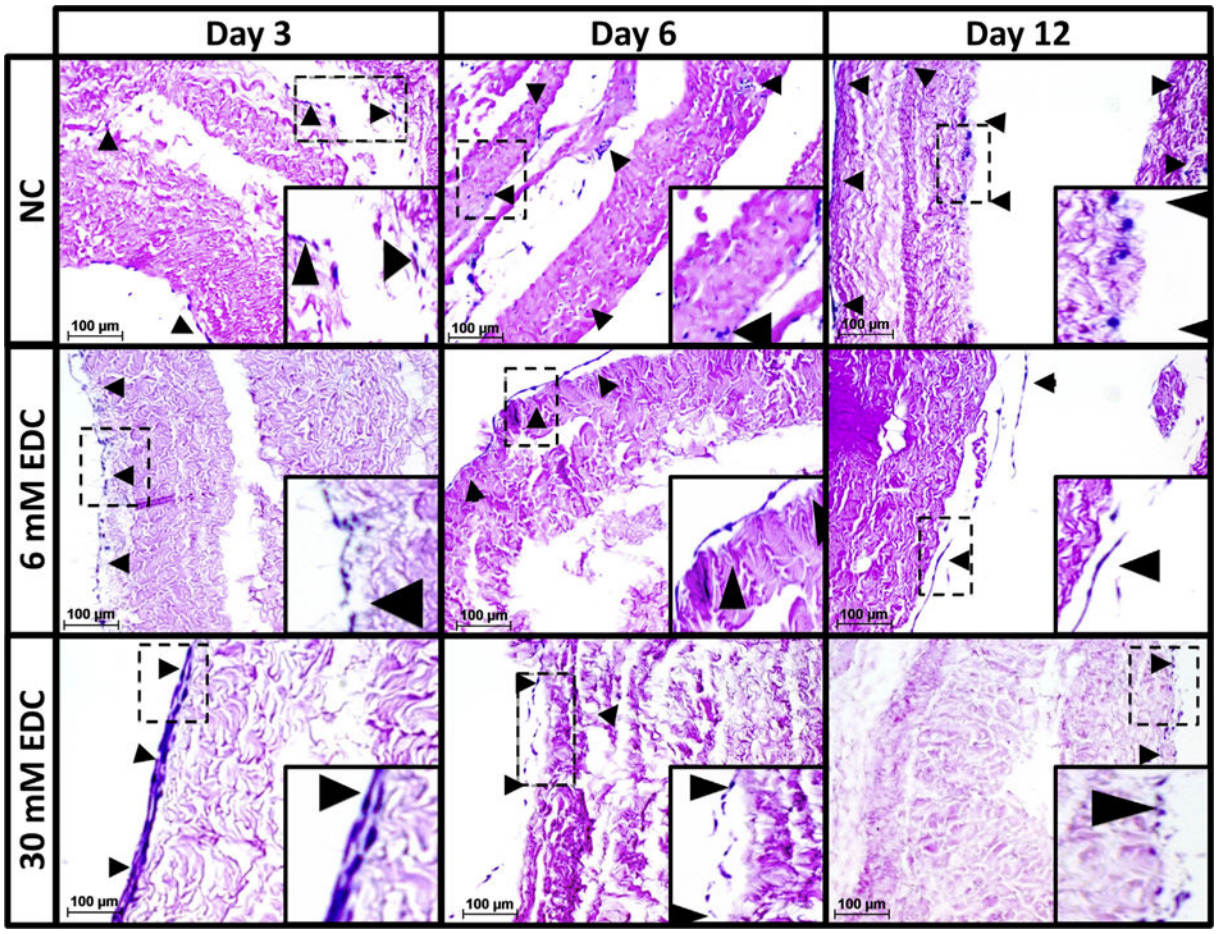

Fig. 7.

Cell infiltration in crosslinked AFRPS. Representative H&E images (200×) of non-crosslinked, 6 mM EDC, and 30 mM EDC AFRPs following cell seeding. Crosslinked samples illustrate minimal cell infiltration into AFRPs in contrast to non-crosslinked samples at respective time points (Insert: Magnified image highlighting representative region of interest outlined by dotted-line). (Black arrow head indicates cell nuclei). (Methods used to generate data within this figure are described in section 2.6.4).

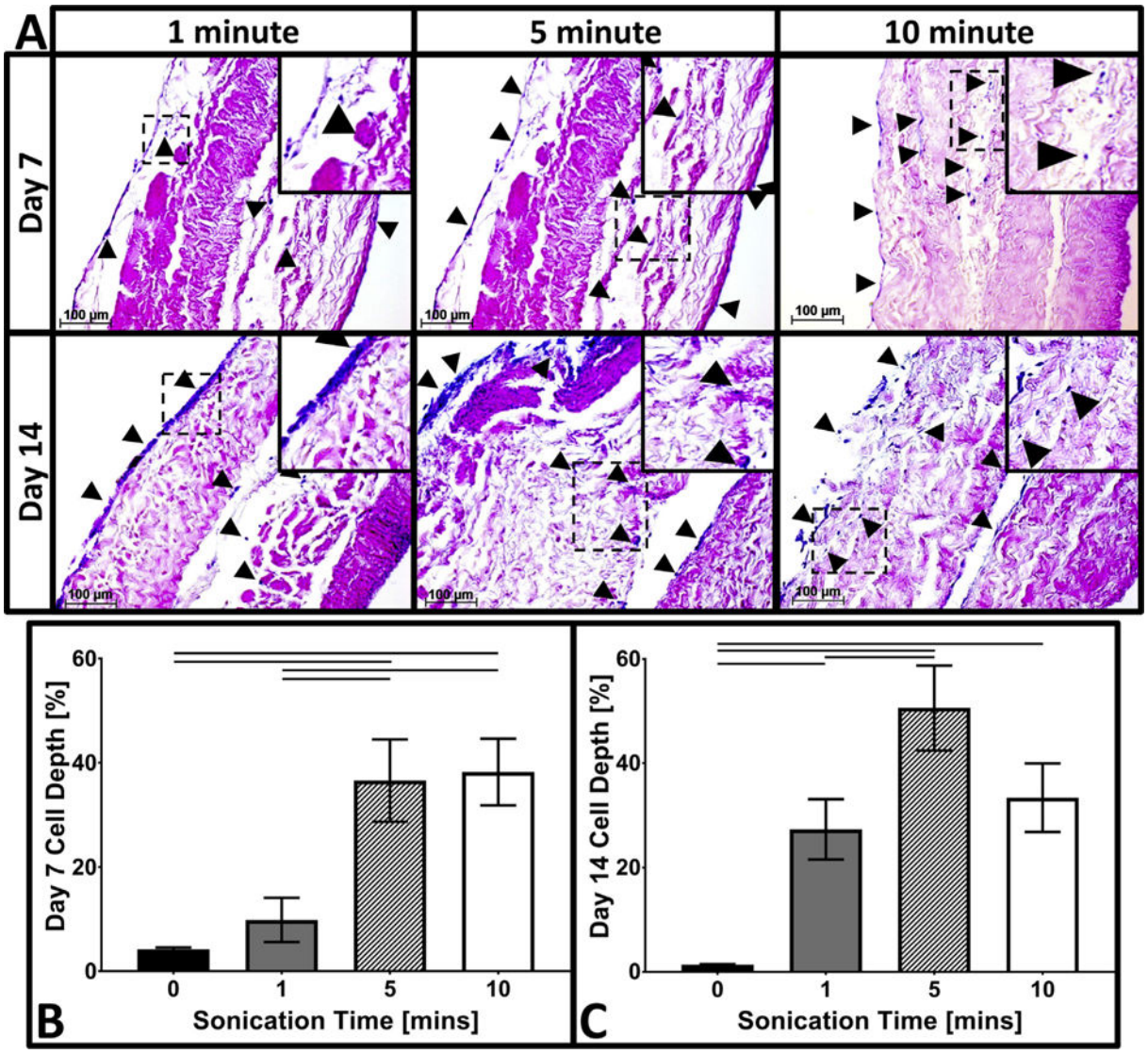

Fig. 8.

Cell infiltration of bAFCs into crosslinked and sonicated AFRPS. A) Representative H&E images (200×) of 6 mM EDC crosslinked AFRPs following 1-, 5-, and 10-min of sonication at the respective time points. (Insert: Magnified image highlighting representative region of interest outlined by dotted-line). (Black arrow head indicates cell nuclei). B–C) Representative graphs of the average cell infiltration depth. Solid connecting lines indicate significant difference ($p < 0.05$). (Methods used to generate data within this figure are described in section 2.6.7).

Table 1

Summary of RoM and slow ramp compression results from kinematic testing.

Cyclic loading					**Slow ramp**
	Compressive Stiffness [N/mm]	**Tensile Stiffness [N/mm]**	**NZ Length [mm]**	**Range of Motion [mm]**	**Compressive Stiffness [N/mm]**
Intact	1120.95 ± 48.64	319.64 ± 31.87	1.63 ± 0.09	4.18 ± 0.17	527.21 ± 20.87
Annulotomy	1009.17 ± 79.4	286.09 ± 16.81	1.76 ± 0.11	4.45 ± 0.15	412.13 ± 46.72
Discectomy	1021.77 ± 101.0	309.68 ± 17.57	1.86 ± 0.09	*__4.62 ± 0.18__	*__324.95 ± 12.90__
Repair	1093.23 ± 43.96	315.79 ± 20.63	1.74 ± 0.11	4.43 ± 0.2	350.72 ± 52.71

*(bold) indicates significant difference ($p < 0.05$) from intact controls. Statistical analysis was performed using a one-way repeated measures ANOVA.

Table 2

Summary of creep results from kinematic testing.

Creep Period						
	Step Disp. [mm]	**Creep Disp. [mm]**	**Short-term response**		**Long-term response**	
			Ψ_1 [N/mm]	**η_1 [Ns/mm]**	**Ψ_2 [N/mm]**	**η_2 [Ns/mm]**
Intact	1.22 ± 0.3	1.45 ± 0.1	765.5 ± 61.9	9.6 ± 0.3	142.6 ± 12.4	46.1 ± 5.2
Annulotomy	2.25 ± 0.2	***1.06 ± 0.1**	749.4 ± 66.6	8.1 ± 0.9	***215.6 ± 15.4**	***72.3 ± 5.3**
Discectomy	2.89 ± 0.5	***1.04 ± 0.1**	***663.9 ± 65.9**	***6.8 ± 0.9**	***254.2 ± 21.9**	***73.2 ± 5.2**
Repair	**^1.61 ± 0.4**	**^1.50 ± 0.1**	***^445.2 ± 55.3**	***^4.9 ± 0.9**	***^197.1 ± 12.7**	**^47.9 ± 2.86**

* (bold) indicates significant difference ($p < 0.05$) to intact controls.

^ (bold) indicates significant difference ($p < 0.05$) between repair and discectomy groups. Statistical analysis was performed using a one-way repeated measures ANOVA.